RSC Advances

PAPER

View Article Online
View Journal | View Issue

Cite this: *RSC Adv.*, 2021, **11**, 953

High efficiency removal of Pb(II) in aqueous solution by a biochar-supported nanoscale ferrous sulfide composite

Chengguang Chen[a] and Muqing Qiu *[b]

Received 21st September 2020
Accepted 21st November 2020

DOI: 10.1039/d0ra08055a

rsc.li/rsc-advances

A biochar-supported nanoscale ferrous sulfide composite was prepared and applied for the treatment of Pb(II) ions in aqueous solution. The experimental results of SEM, EDS, XRD, and FT-IR spectroscopy clearly implied that the biochar was successfully modified with nanoscale ferrous sulfide composite. The maximum adsorption capacity of Pb(II) ions by FeS@biochar reached 88.06 mg g^{-1}. Compared with other reported adsorbents, the removal rate of Pb(II) ions by FeS@biochar was higher. The pseudo-second-order kinetic model and Langmuir isotherm model could better fit the experimental adsorption results. The removal rate of Pb(II) ions by FeS@biochar was controlled by the chemical reaction and monolayer adsorption on the surface of FeS@biochar. The mechanisms of Pb(II) removal from aqueous solutions by biochar involved electrostatic attraction, hydrogen bonding, physical adsorption, ion exchange, and chemical precipitation. Additionally, the chemical stability and reusability of FeS@biochar were good. It is also an environment-friendly material for low-cost wastewater treatment.

Introduction

Lead is a highly toxic heavy metal pollutant. It is also widely present in industrial wastewater.[1,2] In China, metals such as Pb^{2+}, Hg^{2+}, Cd^{2+}, As^{3+}, and Cr^{6+} are listed by the Ministry of Environmental Protection as priority heavy metal pollutants to be controlled.[3,4] Lead, in the environment, mainly comes from acid storage batteries, lead smelting, and oil processing industries. Because the heavy metal lead can bioaccumulate in plants or animals through the food chain, even low concentrations of lead in natural water bodies can cause great harm to human health and the ecological environment. Therefore, lead-containing wastewater must be effectively treated before being discharged.[5] At present, the main methods for the treatment of lead-containing wastewater include chemical precipitation method,[6,7] ion exchange method,[8] electrochemical method,[9] and adsorption method.[10–12] However, the adsorption method is widely applied for water treatment because of its simple operation and low cost.

In recent years, biochar prepared from waste biomass under high temperature and oxygen-limited conditions has been extensively researched for its advantages, such as low price, simple preparation process, and a wide range of precursor sources.[13–18] However, biochar has poor adsorption capacity.[19,20] In addition, its separation from solid–liquid mixtures is difficult. Therefore, some scholars have paid attention to the combined composites of biochar and other materials. Some physical and chemical methods were applied to prepare new materials, by combining biochar with other materials. These new composites, such as magnetic biochar,[21–24] graphene@biochar,[25] nano-zero valent iron@biochar,[26–29] and carbon nanotubes@biochar,[30] have been widely used in the research of Pb^{2+} adsorption from aqueous solutions.

Iron–sulfur compounds (FeS, FeS_2, *etc.*) can effectively stabilize divalent metals (Co^{2+}, Cu^{2+}, Ni^{2+}, Mg^{2+}, *etc.*) due to their surface chemistry and unique molecular structure. These compounds contain a lot of Fe^{2+} ions and S_x^{2-} ions. Both of these ions can serve as effective electron donors and provide good reducibility. It could provide a lot of Fe^{2+} ions and S_x^{2-} ions to facilitate heavy metal reduction. Lu *et al.* investigated the effectiveness of natural FeS minerals for the removal of Cr(VI) ions in solution. It indicated that natural FeS minerals removed greater.[31]

At the same time, iron–sulfur compounds are inexpensive, easy to prepare, and generally do not cause secondary pollution. They can be effectively applied to contaminated water bodies and soil remediation.[32–36] However, the small size and extremely high surface energy make FeS_x compounds to agglomerate easily, leading to poor stability and easy deactivation. Therefore, stabilization measures must be taken to improve their removal effect in practical engineering applications.

In this study, a new biochar modified by iron sulfide particles (FeS@biochar) was prepared. Then, the elimination of Pb(II) ions by this material was tested. This study highlighted the high stability and efficient removal rate of Pb(II) ions by FeS@biochar making it a potential adsorbent for the cleanup of

[a]*School of Architectural Engineering, Shaoxing University, Yuanpei College, Shaoxing, 312000, P. R. China. E-mail: qiumuqing@126.com*
[b]*School of Life Science, Shaoxing University, Shaoxing, 312000, P. R. China*

environmental pollutants. The main objectives were to: (1) prepare a new material, FeS@biochar; (2) to characterize this material through microscopic technologies; (3) test the effects of operational parameters on the removal of Pb(II) ions by adsorption experiments; and (4) elaborate the reaction mechanism of Pb(II) in aqueous solution and FeS@biochar in detail.

Materials and methods

Chemicals

All chemicals used in this experiment were of analytical grade. Chitosan, ferrous sulfate heptahydrate ($FeSO_4 \cdot 7H_2O$), sodium sulfide nonahydrate ($Na_2S \cdot 9H_2O$), and lead nitrate ($Pb(NO_3)_2 \cdot 6H_2O$) were obtained from Sinopharm Chemical Reagent Co., Ltd. (Shanghai, China). Peanut shells were obtained from a farm in Jinan City, Shandong Province, China. Anaerobic deionized water was obtained by aerating N_2 into deionized water for over 30 min under magnetic stirring. This anaerobic deionized water was used in all the experiments.

Preparation of adsorbents

The peanut shells were rinsed with deionized water three times, then transferred into an oven and heated for 24 h at 110 °C. After cooling down, the dried peanut shells were crushed into 1–2 cm pieces and carbonized for 2 h at 250 °C in a muffle furnace. Then, the biochar was pulverized and sieved through a 60 mesh sieve. Thus, biochar from peanut shells was obtained.

The iron-sulfide nanoparticles (FeS) were prepared by the reaction of $FeSO_4$ with Na_2S, in which 50 mL $FeSO_4$ solution (0.05 mol L^{-1}) was added into a 250 mL Erlenmeyer flask containing 50 mL Na_2S solution (0.05 mol L^{-1}), followed by mixing for 30 min under continuous N_2 aeration and magnetic stirring conditions. The suspensions were then sealed and aged for 24 h. Finally, the iron-sulfide nanoparticles were obtained for experiments.

FeS@biochar was prepared according to the method reported by Lyu *et al.*[37] In this research, it was found that the composite material prepared by keeping the mass ratio of biochar and iron sulfide nanoparticles at 4 : 1 had the best adsorption performance for Pb^{2+} ions in aqueous solution. 7.91 g of $FeSO_4 \cdot 7H_2O$ was dissolved in 100 mL anaerobic deionized water under continuous N_2 aeration and magnetic stirring conditions. Then, 10 g of the biochar derived from peanut shells was added to the above $FeSO_4$ solution and stirred for 10 min. Subsequently, 6.82 g of $Na_2S \cdot 9H_2O$ was also added to the above mixture and stirred for 20 min. The entire preparation process was under continuous N_2 aeration and magnetic stirring conditions. The suspension was then sealed and aged for 24 h. The mixture was freeze-dried, washed with anaerobic deionized water three times, and freeze-dried again. Finally, the novel FeS@biochar material was obtained for subsequent experiments.

Characterization of adsorbents

The surface morphology and structure of the adsorbents were observed with SEM (JEOL 6500F, Japan). A surface area and pore size analyzer (Quantachrome, FL, USA) was used to determine the surface area and pore size of the adsorbents at a relative pressure of 0.95 following the multipoint N_2-BET adsorption method. The crystalline structures of the adsorbents were studied using a D/Max-IIIA Powder X-ray Diffractometer (Rigaku Corp., Japan). The surface functional groups of the adsorbents were investigated by using a Nexus 670 FTIR spectrometer (Thermo Nicolet, Madison) in the wave number range of 500–4000 cm^{-1}. An XPS (X-ray photoelectron spectrometer, Krato AXIS Ultra DLD, Japan) and the model Axis-HS (Kratos Analytical) were used to determine the surface composition.

Adsorption experiments

All experiments were carried out on a shaker at 200 rpm under a constant temperature condition. Firstly, the adsorbent was added to 100 mL Pb(II) in a 250 mL Erlenmeyer flask. The flask was then sealed by a bottle cap and placed in the shaker at 200 rpm and constant temperature. The pH of the solution was adjusted by 0.1 mol L^{-1} HCl or NaOH solution. The entire adsorption process reached equilibrium, and the supernatant was collected through filtration. The Pb(II) concentration was determined by UV-vis spectrophotometry. The residual sample was centrifuged at 4000 rpm for 15 min, and the sediment was investigated by microscopic technologies. The removal rate (R) and the uptake capacity (q) were calculated using eqn (1) and (2).

$$R = (C_0 - C_e) \times 100\%/C_0 \quad (1)$$

$$q = (C_0 - C_e) \times V/m \quad (2)$$

where C_0 (mg L^{-1}) and C_e (mg L^{-1}) are the initial concentration and equilibrium concentration, respectively. V (L) is the solution volume, and m (g) is the weight of the adsorbent.

Results and discussion

Characterization of adsorbents

The surface area and pore size of biochar and FeS@biochar were determined by the surface area and pore size analyzer. The results showed that the BET specific surface area of the biochar and FeS@biochar were 65.15 and 82.73 $m^2\ g^{-1}$, respectively. The adsorption average pore width of biochar and FeS@biochar were 4.1 and 17.2 nm, respectively. Because the FeS nanoparticles were loaded onto the surface of biochar, both the

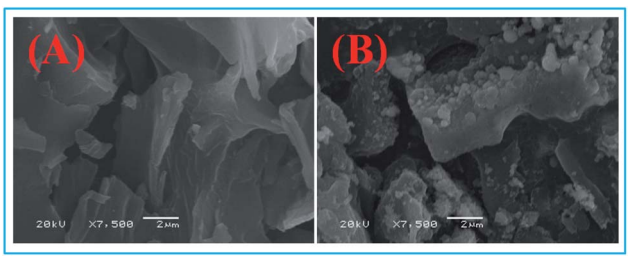

Fig. 1 SEM images of (A) biochar and (B) FeS@biochar.

surface area and pore size of biochar increased. SEM and TEM images of biochar and FeS@biochar are displayed in Fig. 1.

As shown in Fig. 1A, it could be deduced that the surface of the obtained biochar was smooth with irregular structure. On the other hand, the surface of FeS@biochar (Fig. 1B) was rough and contained a lot of fine particles. Additionally, a lot of flocculent substances were observed on the surface of biochar, which implies that the dispersion of FeS nanoparticles occurred on its surface. This result was consistent with the TEM images of biochar and FeS@biochar (Fig. 2). It could be observed that the size of FeS nanoparticles was 21.52 nm, and the surface of biochar was covered by FeS nanoparticles.

This structure would facilitate the adsorption of pollutants. Moreover, it could also be inferred from this result that FeS nanoparticles were successfully loaded on the surface of biochar, which could be further verified from the EDS spectrum of biochar and FeS@biochar (Fig. 3).

The elements present in biochar (Fig. 2A) were mainly C, O, K, and Ca, and their contents were 71.97, 25.77, 1.46, and 0.80%, respectively. The elements present in FeS@biochar (Fig. 2B) were mainly C, O, S, Na, and Fe, and their contents were 52.20, 38.26, 1.43, 1.62, and 6.49%, respectively. However, the oxygen content of the synthesized FeS@biochar was relatively high due to the presence of oxygen in the process of FeS@biochar synthesis. The appearance of Fe and S elements suggested that they were mainly from FeS nanoparticles. Additionally, the composite material was prepared by keeping the mass ratio of biochar and FeS nanoparticles at 4 : 1. It could be observed that the contents of Fe and S in the prepared composite materials (FeS@biochar) were lower than the theoretical value. It might be because a part of FeS nanoparticles was not supported on the surface of the biochar.

The XRD patterns and FT-IR spectra of biochar and FeS@biochar are displayed in Fig. 4.

The diffraction peaks of biochar (2θ = 20.41°) (Fig. 4A) appeared in the XRD patterns of FeS@biochar. There were eight diffraction peaks (2θ = 14.86, 18.96, 23.32, 27.91, 27.98, 28.94, 32.04, and 33.85°), and they were characteristic peaks of FeS nanoparticles. The FT-IR spectra of biochar and FeS@biochar are shown in Fig. 4B. From Fig. 4B, it could be observed that the characteristic peak of biochar appeared at 2385 cm^{-1} and 2328 cm^{-1}, which could be attributed to the vibrations of C≡C and O=C=O functional group, respectively. However, these peaks disappeared when the biochar was loaded with FeS

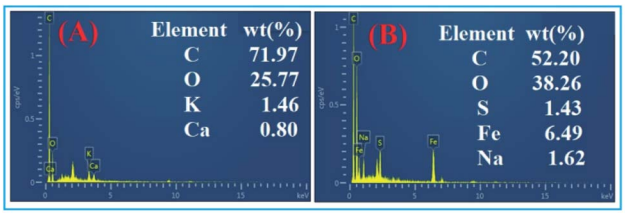

Fig. 3 The EDS spectrum of (A) biochar and (B) FeS@biochar.

nanoparticles. This might be caused by interactions between the molecules. The five characteristic peaks at 2021, 1614, 1380, 1085, and 571 cm^{-1} appeared for biochar, and they were assigned to the vibrations of –C=C=N,C=O, O=C–O, and –C–H functional groups, respectively. All the characteristic peaks of biochar appeared in the case of FeS@biochar as well.

Adsorption experiments

To elucidate the adsorption process and reaction mechanisms, the effects of operational parameters on the removal of Pb^{2+} ions in aqueous solution by adsorbents were tested. The experimental conditions were as follow: C_0 = 60 mg L^{-1}, dosage = 0.05 g, solution volume = 100 mL, pH = 4.7, T = 308 K, contact time of 360 min, and rotating speed = 200 rpm. The experimental results are displayed in Fig. 5.

As observed in Fig. 5A, the adsorption process of Pb(II) ions could be divided into two stages. One was the fast stage of the adsorption process, and the other was the slow stage of the adsorption process. In the first stage of the adsorption process, the removal rate of Pb(II) ions increased quickly with an increase in the contact time. This stage was the fast stage of the adsorption process. In this stage, the removal rate of Pb(II) ions from the solution by FeS@biochar reached 75.21% within 30 min. However, with further increase in the contact time, the removal rate increased slowly. Thus, the adsorption process entered a slow stage. In this stage, the removal rate reached 80.79% in 360 min. The effect of the initial concentration and temperature are shown in Fig. 5B and D, respectively. The removal rate of Pb(II) by FeS@biochar decreased with an increase in the initial concentration. Additionally, the removal rate of Pb(II) by FeS@biochar decreased with the increasing temperature. The pH of the solution was an important factor affecting the adsorption capacity. It not only determined the

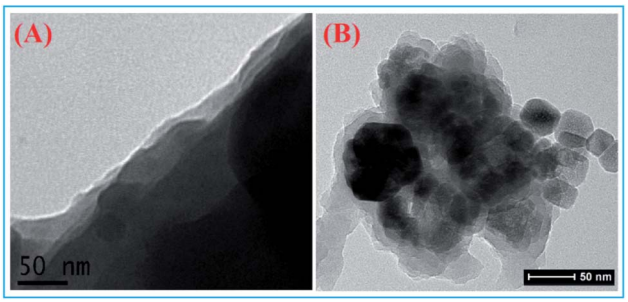

Fig. 2 TEM images of (A) biochar and (B) FeS@biochar.

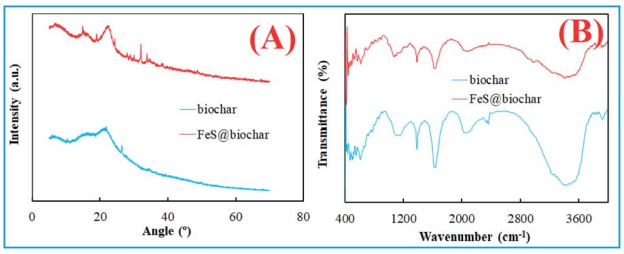

Fig. 4 The XRD patterns (A) and FT-IR spectra (B) of biochar and FeS@biochar.

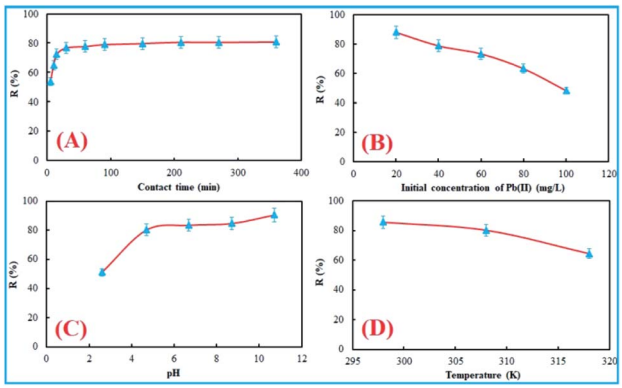

Fig. 5 Effects of contact time (A), initial concentration of Pb(II) (B), pH (C), and temperature (D) on the removal rate of Pb(II) by FeS@biochar.

surface charge of the adsorbent but also affected the existent form of heavy metal ions. The results of the experiment are displayed in Fig. 5C. The removal rate of Pb(II) ions by FeS@biochar increased when the pH was increased. When pH > 4, the increasing trend of the removal rate was flattening, and the removal rate reached more than 80.21%. However, when the pH was further increased, the increase in the removal rate was very less. At 150 minutes, it basically reached the state of adsorption equilibrium. In short, the operational parameters had an important influence on the removal rate of Pb(II) ions by FeS@biochar.

Adsorption kinetics, adsorption isotherm and thermodynamics

Pseudo-first-order kinetic model (eqn (3))[38] and pseudo-second-order kinetic model (eqn (4))[39] were used to describe the adsorption kinetics of Pb(II) ions in solution by FeS@biochar.

$$\ln(q_e - q_t) = \ln q_e - k_1 t \quad (3)$$

$$\frac{1}{q_e - q_t} = \frac{1}{q_e} + k_2 t \quad (4)$$

where k_1 and k_2 are the pseudo-first-order rate constant (min^{-1}) and the pseudo-second-order rate constant (g mg^{-1} min^{-1}), respectively. q_e and q_t are the adsorption amount of Pb(II) ions at equilibrium and at any time t (mg g^{-1}), respectively.

The adsorption isotherm was described by the Langmuir model (eqn (5))[40] and the Freundlich model (eqn (6)).[41]

$$q_e = \frac{q_{max} b C_e}{1 + b C_e} \quad (5)$$

$$q_e = K C_e^{\frac{1}{n}} \quad (6)$$

where b is the Langmuir constant (L mg^{-1}), and K and $1/n$ are the Freundlich constants. K indicates the relative adsorption capacity, while $1/n$ indicates the intensity of the adsorption. C_e is the equilibrium concentration of the solute (mg L^{-1}), and q_{max} is the maximum adsorption capacity (mg L^{-1}).

In order to further explore the mechanism of Pb(II) uptake, thermodynamic parameters, such as Gibbs free energy (ΔG^0 (kJ mol^{-1})), enthalpy (ΔH^0 (kJ mol^{-1})), and entropy (ΔS^0 (J mol^{-1} K^{-1})), were evaluated to determine the spontaneity of the reaction. They were associated with the adsorption and can be calculated using the following eqn (7)–(9):[42]

$$\Delta G^0 = -RT \ln K_a \quad (7)$$

$$\ln K_a = \frac{\Delta S^0}{R} - \frac{\Delta H^0}{RT} \quad (8)$$

$$K_a = \frac{q_e}{C_e} \quad (9)$$

where T is the solution temperature (K), K_a is the adsorption equilibrium constant, R is the gas constant (8.314 J mol^{-1} K^{-1}), q_e is the amount of adsorbate adsorbed per unit mass of adsorbent at equilibrium (mg g^{-1}), and C_e is the equilibrium concentration of the adsorbate (mg L^{-1}). ΔS^0 and ΔH^0 were calculated from the slope and the intercept, respectively.

Using the data from Fig. 5A, the adsorption kinetics for Pb(II) ions in solution by FeS@biochar are displayed in Fig. 6Aand B. It could be suggested that adsorption processes were fitted with the pseudo-second-order kinetic model by comparing the value of R^2 (0.9987 > 0.8793). In other words, the adsorption processes of Pb(II) ions by FeS@biochar could be described by the pseudo-second-order kinetic model. The removal rate of Pb(II) ions by FeS@biochar was controlled by the chemical reaction that occurred on the surface of FeS@biochar. Using the data from Fig. 5B, the adsorption isotherms for Pb(II) ions in solution by FeS@biochar are shown in Fig. 6C and D. As shown in Fig. 6C and D, the Langmuir isotherm model ($R^2 = 0.9921$) could better fit the experimental adsorption results. It also described that the adsorption processes of Pb(II) ions by FeS@biochar mainly involved monolayer adsorption on the surface of FeS@biochar. The maximum adsorption capacity of Pb(II) ions by FeS@biochar reached 88.06 mg g^{-1}.

The adsorption performance of FeS@biochar and other reported adsorbents for Pb(II) ion removal was compared. The results are listed in Table 1.

The removal rate of Pb(II) was high. Using the data from Fig. 5D and eqn (7)–(9), thermodynamic parameters were

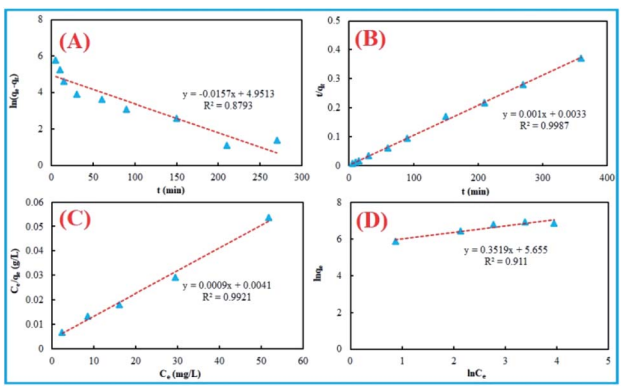

Fig. 6 The kinetic adsorption (pseudo-first-order kinetic model (A) and pseudo-second-order kinetic model (B)) and adsorption isotherms (Langmuir isotherm model (C) and Freundlich isotherm model (D)) for Pb(II) ions in solution by FeS@biochar.

calculated and are listed in Table 2. The value of ΔG^0 increased with an increase in the reaction temperature. It reflected that the low reaction temperature was beneficial for Pb(II) ion uptake. The negative value of ΔG^0 depicted that Pb(II) ion uptake was spontaneous. The negative value of ΔH^0 indicated that the interaction of Pb(II) ions with FeS@biochar was an exothermic chemical reaction. The negative value of ΔS^0 indicated the existence of some structural changes at the adsorbent–solution interface. In short, the uptake process of Pb(II) ions in solution by FeS@biochar was a spontaneous and exothermic chemical reaction process.

Table 2 Thermodynamic parameters of Pb(II) ion uptake capacity by FeS@biochar under different temperatures

ΔG^0 (kJ mol^{-1})			ΔH^0 (kJ mol^{-1})	ΔS^0 (J mol^{-1} K^{-1})	R^2
298 (K)	308 (K)	318 (K)			
−11.84	−11.25	−9.49	−46.57	−115.92	0.9521

Adsorption mechanism

In order to investigate the mechanism of Pb(II) removal by FeS@biochar, the sample of FeS@biochar was studied by XPS, and the results are shown in Fig. 7.

The sample of FeS@biochar exhibited four characteristic peaks, with binding energies of 169.15, 285.26, 532.19, and 711.7 eV. They were ascribed to S 2p, C 1s, O 1s, and Fe 2p, respectively. Moreover, their atomic weight was 3.98, 2.51, 59.2, and 32.66%, respectively. The elements Fe and S appeared in the spectra of FeS@biochar. This confirmed that biochar was successfully loaded with FeS nanoparticles. After the adsorption of Pb(II) by FeS@biochar, the Pb 4f peak was observed in the survey spectra of FeS@biochar. The atomic weight of Pb reached 0.25%. It indicated that Pb was successfully adsorbed by FeS@biochar and appeared on the surface of FeS@biochar. As displayed in Fig. 7B, the Pb 4f spectrum exhibited two characteristic peaks at 139.05 and 143.95 eV. They were ascribed to Pb $4f_{7/2}$ and Pb $4f_{5/2}$, respectively. In short, the Pb 4f spectrum provided evidence on the interaction between Pb(II) and FeS@biochar. The result is in agreement with adsorption experiments. In Fig. 7C and D, one can observe that the high-resolution spectra of Fe 2p and S 2p exhibited changes in the intensity of Fe and S peaks before and after the reaction with Pb(II) ions. The high-resolution spectra of Fe 2p exhibited two characteristic peaks at 711.6 eV and 725.1 eV before the reaction with Pb(II) ions. After the adsorption of Pb(II) ions, the two characteristic peaks changed very little. However, one characteristic peak in the S 2p spectrum disappeared after the adsorption of Pb(II) ions. It indicated that FeS nanoparticles underwent a redox reaction with Pb(II). In other words, Pb(II) ions in the solution were removed by FeS@biochar through adsorption and redox reaction.

The mechanism of decontamination by FeS nanoparticles was studied in detail.[43]

$$FeS \Leftrightarrow Fe^{2+} + S^{2-} \quad (10)$$

$$S^0(s) + 2e^- \Leftrightarrow S^{2-} \quad (11)$$

$$S^0(s) + H^+ + 2e^- \Leftrightarrow HS^- \quad (12)$$

$$S^0(s) + 2H^+ + 2e^- \Leftrightarrow H_2S(g) \quad (13)$$

$$H_2SO_3 + 4H^+ + 4e^- \Leftrightarrow S + 3H_2O \quad (14)$$

$$SO_4^{2-} + H_2O + 2e^- \Leftrightarrow SO_3^- + 2OH^- \quad (15)$$

Therefore, based on SEM images, XRD patterns, EDS spectrum, FT-IR spectra, XPS spectra, and adsorption experiments, a proposed reaction mechanism for the removal of Pb(II) by FeS@biochar is displayed in Fig. 8.

As shown in Fig. 8, the proposed reaction mechanism for the capture of Pb(II) by FeS@biochar is as follow: oxygen containing functional groups (such as –C=C=N, C=O, O=C–O, and –C–H functional group) in FeS@biochar would result in negative charges on the surface of FeS@biochar. Therefore, they could effectively form a complex with Pb(II).[44] Additionally, FeS could

Table 1 The comparison of the adsorption performance of FeS@-biochar with that of the other reported adsorbents for Pb(II) ion removal

Sorbent	q_{max} (mg g^{-1})	Reference
Biochar from maple wood	43.3	11
Biochar from pine wood	3.89	12
Sweetgum biochar supported with GO	40	13
Activated carbon	30.46	14
Piegeon peas hulls	20.83	15
Modified hydrochar from peanut hull	22.82	16
Modified cotton	69.5	17
Carbon nanotubes	17.44	18
Fes@biochar	88.06	This work

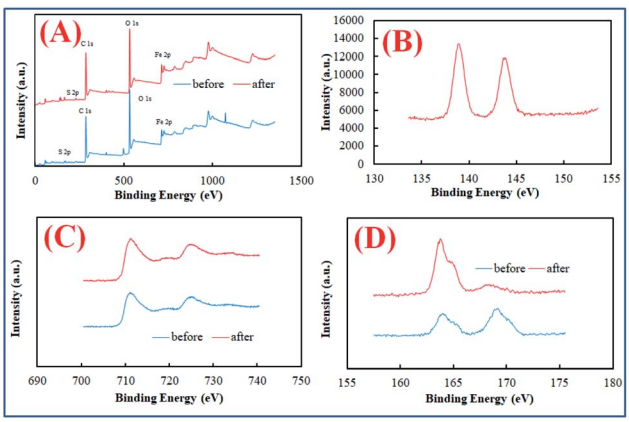

Fig. 7 XPS analysis of FeS@biochar before and after the reaction with Pb(II) ions ((A) survey spectra of FeS@biochar; (B) high-resolution spectra of Pb 4f; (C) high-resolution spectra of Fe 2p, and (D) high-resolution spectra of S 2p).

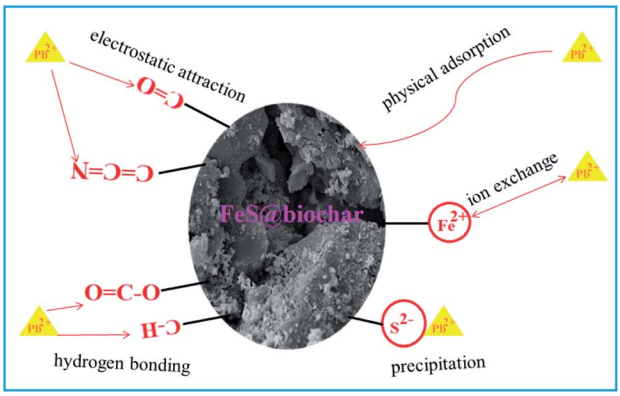

Fig. 8 The proposed reaction mechanism for the capture of Pb(II) by FeS@biochar.

react with Pb(II). As a result, Pb(II) could be precipitated as PbS. Therefore, the mechanisms of Pb(II) removal by biochars also involved electrostatic attraction, hydrogen bonding, physical adsorption, and ion exchange in addition to chemical precipitation.[44]

Recycling experiments

The use of recycled adsorbent is very important in practical applications. In order to investigate the performance of recycled FeS@biochar, a series of experiments were carried out. The experimental conditions were as follow: $C_0 = 60$ mg L^{-1}, dosage = 0.05 g, solution volume = 100 mL, pH = 4.7, $T = 308$ K, contact time of 360 min, and rotating speed = 200 rpm. FeS@biochar after adsorbing Pb(II) ions was treated by the following method. It was soaked in 250 mL flasks containing 100 mL 0.1 mol L^{-1} NaOH for 30 min, and washed by 100 mL Milli-Q water. It was then soaked in 250 mL flasks containing 100 mL 0.1 mol L^{-1} HCl for 30 min again. Subsequently, it was washed by 100 mL of Milli-Q water again. The use of recycled FeS@biochar was plotted and displayed in Fig. 9. It depicted that the removal rate of Pb(II) ions reached 75.89% in the first use. When the reuse time was increased, the removal rate of Pb(II) ions decreased. However, the uptake capacity of Pb(II) ions still reached 58.12% in the fourth recycle run. It indicated that the chemical stability and reusability of FeS@biochar were good. It is also an environment-friendly material for low-cost wastewater treatment.

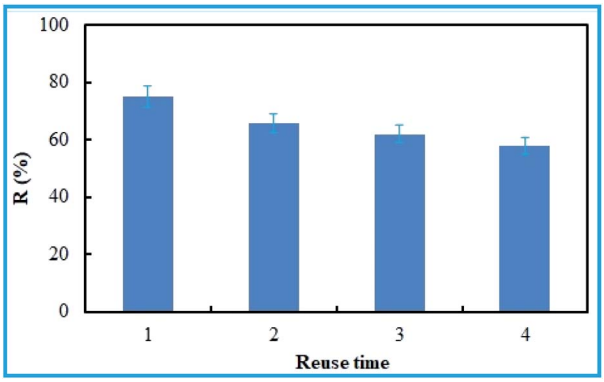

Fig. 9 The use of recycled FeS@biochar for uptake of Pb(II) ions in solution.

Conclusions

A new type of biochar modified by iron-sulfide particles was prepared. Then, the removal of Pb(II) by this material was tested. The surface of FeS@biochar was rough and contained a lot of fine particles. The pseudo-second-order kinetic model (R^2 = 0.9987) and Langmuir isotherm model (R^2 = 0.9921) could better fit the experimental adsorption results. The removal rate of Pb(II) ions by FeS@biochar was controlled by the chemical reaction and monolayer adsorption on the surface of FeS@biochar. The reaction mechanism for capture of the Pb(II) removal by FeS@biochar was suggested. FeS@biochar exhibited good chemical stability and reusability in the treatment of wastewater containing Pb(II) ions.

Conflicts of interest

We declare that we have no financial and personal relationships with other people or organizations that could inappropriately influence this work. There was no professional or other personal interest of any nature or kind in any product, service and/or company that could be construed as influencing the position presented in, or the review of, the manuscript entitled, "High efficiency removal of Pb(II) in aqueous solution by a biochar-supported nanoscale ferrous sulfide composite".

Acknowledgements

This work was financially supported by the National Natural Science Foundation of China (No. 21876115) and Natural Science Foundation of Zhejiang Province, China (LGF20C030001). The authors were very grateful for the support. C. G. Chen (Associate Professor) conducted all the experiments and wrote the manuscript. M. Q. Qiu (Professor) revised the manuscript.

Notes and references

1 R. K. Gautam, A. Mudhoo, G. Lofrano and M. C. Chattopadhyaya, *J. Environ. Chem.*, 2013, **2**, 239.
2 K. S. Arum, A. Javed, A. Mansour, A. D. Lawrence, A. A. A. Fekri, M. R. Muthumareeswaran, M. Umesh and A. A. Mohammad, *Environ. Sci.: Water Res. Technol.*, 2018, **4**, 438.
3 A. R. Graham, H. M. Dan, J. B. Stephen, J. R. Thomas and N. K. Andrei, *Mater. Chem. Phys.*, 2019, **233**, 102.
4 L. J. Dong, Z. L. Zhu, Y. L. Qiu and J. F. Zhao, *Chem. Eng. J.*, 2010, **165**, 827.
5 H. Wang, N. C. Yang and M. Q. Qiu, *J. Inorg. Mater.*, 2020, **35**, 301.
6 M. Q. Qiu, M. Wang, Q. Z. Zhao, B. W. Hu and Y. L. Zhu, *Chemosphere*, 2018, **201**, 764.

7 C. Oh, Y. S. Han and J. H. Park, *Sci. Total Environ.*, 2016, **557**, 212.
8 B. L. Rivas, B. Urbano, S. A. Pooley, I. Bustos and N. Escalona, *Polym. Bull.*, 2012, **68**, 1577.
9 M. C. Shinzato, T. J. Montanheiro and V. A. Janasi, *Environ. Earth Sci.*, 2012, **66**, 363.
10 P. Tan, J. Sun and Y. Hu, *J. Hazard. Mater.*, 2015, **297**, 251.
11 M. Inyang, B. Gao, A. Zimmerman, M. Zhang and H. Chen, *Chem. Eng. J.*, 2014, **236**, 39.
12 M. Inyang, B. Gao, A. Zimmerman, Y. M. Zhou and X. D. Cao, *Environ. Sci. Pollut. Res.*, 2014, **22**, 1868.
13 Q. Wang, B. Wang, X. Q. Lee, J. Lehmann and B. Gao, *Sci. Total Environ.*, 2018, **634**, 188.
14 Z. Liu and F. S. Zhang, *J. Hazard. Mater.*, 2009, **167**, 933.
15 T. Liu, B. Gao, J. Fang, B. Wang and X. Cao, *RSC Adv.*, 2016, **6**, 24314.
16 K. Kadirvelu, C. Faur-Brasquet and P. L. Cloirec, *Langmuir*, 2000, **16**, 8404.
17 R. D. K. Venkata, K. R. D. Harikishore, J. S. Yu and K. Seshaiah, *Chem. Eng. J.*, 2012, **197**, 24.
18 Y. Xue, B. Gao and Y. Yao, *Chem. Eng. J.*, 2012, **200–202**, 673.
19 Z. Ding, X. Hu, A. R. Zimmerman and B. Gao, *Bioresour. Technol.*, 2014, **167**, 569.
20 Y. H. Li, S. Wang and J. Wei, *Chem. Phys. Lett.*, 2002, **357**, 263.
21 X. Huang, D. Wei and X. W. Zhang, *Sci. Total Environ.*, 2019, **685**, 681.
22 M. R. Chandraiah, *Alexandria Eng. J.*, 2016, **55**, 619.
23 S. Y. Wang, Y. K. Tang, C. Chen, J. T. Wu, Z. N. Huang, Y. Y. Mo, K. X. Zhang and J. B. Chen, *Bioresour. Technol.*, 2015, **186**, 360.
24 R. H. Li, H. X. Deng, X. F. Zhang, J. J. Wang, M. K. Awasthi, Q. Wang, R. Xiao, B. Y. Zhou, J. Du and Z. Q. Zhang, *Bioresour. Technol.*, 2019, **273**, 335.
25 Y. Zhang, B. Cao, L. L. Zhao, L. L. Sun, Y. Gao, J. J. Li and F. Yang, *Appl. Surf. Sci.*, 2018, **427**, 147.
26 A. Mitzia, M. Vítková and M. Komárek, *Chemosphere*, 2020, **242**, 125248.
27 L. B. Qian, S. N. Liu, W. Y. Zhang, Y. Chen, D. Ouyang, L. Han, J. C. Yan and M. F. Chen, *J. Colloid Interface Sci.*, 2019, **533**, 428.
28 S. S. Wang, B. Gao, Y. C. Li, A. E. Creamer and F. He, *J. Hazard. Mater.*, 2017, **322**, 172.
29 F. Yang, S. S. Zhang, Y. Q. Sun, K. Cheng, J. S. Li and D. C. W. Tsang, *Bioresour. Technol.*, 2018, **265**, 490.
30 C. Zhang, W. J. Wang, A. Duan, G. M. Zeng, D. L. Huang, C. Lai, X. F. Tan, M. Cheng, R. Z. Wang, C. Y. Zhou, W. P. Xiong and Y. Yang, *Chem. Phys. Lett.*, 2020, **739**, 136972.
31 A. H. Lu, S. J. Zhong, J. Chen, J. X. Shi, J. L. Tang and X. Y. Lu, *Environ. Sci. Technol.*, 2006, **40**, 3064.
32 X. P. Wei, H. Yin, H. Peng, R. X. Chen, G. N. Lu and Z. Dang, *Environ. Pollut.*, 2019, **253**, 161.
33 E. Sathiyaraj, S. Thirumaran, S. Ciattini and S. Selvanayagam, *Inorg. Chim. Acta*, 2019, **498**, 119162.
34 H. Wu, L. Li and K. K. Chang, *J. Environ. Chem. Eng.*, 2020, **8**, 103882.
35 M. Y. Sun, G. H. Cheng, X. L. Ge, M. D. Chen, C. Wang, L. P. Lou and X. H. Xu, *Sci. Total Environ.*, 2018, **621**, 1074.
36 Y. Y. Gong, J. C. Tang and D. Y. Zhao, *Water Res.*, 2016, **89**, 309.
37 H. D. Lyu, J. C. Tang, Y. Huang, L. S. Gai, K. Liber and Y. Y. Gong, *Chem. Eng. J.*, 2017, **322**, 516.
38 W. S. Hummers and R. E. Offeman, *J. Am. Chem. Soc.*, 1958, **80**, 1339.
39 S. Lagergren, *Handlingar*, 1898, **24**, 1.
40 I. Langmuir, *J. Am. Chem. Soc.*, 1918, **40**, 1361.
41 H. M. F. Freundlich, *J. Phys. Chem.*, 1906, **57**, 385.
42 J. Duan, H. D. Ji and W. Liu, *Chem. Eng. J.*, 2019, **359**, 1617.
43 S. H. Ho, S. Zhu and J. S. Chang, *Bioresour. Technol.*, 2017, **246**, 123.
44 M. I. Inyang, B. Gao, Y. Yao, Y. W. Xue, A. Zimmerman, A. Mosa, P. Pullammanappallil, Y. S. OK and X. D. Cao, *Crit. Rev. Environ. Sci. Technol.*, 2016, **46**, 406.